Monthly Notices
of the
ROYAL ASTRONOMICAL SOCIETY

MNRAS **439,** 2813–2821 (2014)
Advance Access publication 2014 February 24

doi:10.1093/mnras/stu136

Optical phase coherent timing of the Crab nebula pulsar with Iqueye at the ESO New Technology Telescope

L. Zampieri,[1⋆] A. Čadež,[2] C. Barbieri,[3] G. Naletto,[4,5] M. Calvani,[1] M. Barbieri,[1,3] E. Verroi,[3,4] P. Zoccarato[6] and T. Occhipinti[7]

[1]*INAF-Astronomical Observatory of Padova, I-35122 Padova, Italy*
[2]*Faculty of Mathematics and Physics, University of Ljubljana, 1000 Ljubljana, Slovenia*
[3]*Department of Physics and Astronomy, University of Padova, I-35131 Padova, Italy*
[4]*Department of Information Engineering, University of Padova, I-35131 Padova, Italy*
[5]*CNR-IFN UOS Padova LUXOR, I-35131 Padova, Italy*
[6]*Trimble Terrasat GmbH, Höhenkirchen-Siegertsbrunn, D-85635 Munich, Germany*
[7]*Adaptica s.r.l., I-35129 Padova, Italy*

Accepted 2014 January 17. Received 2014 January 17; in original form 2013 August 20

ABSTRACT

The Crab nebula pulsar was observed in 2009 January and December with a novel very fast optical photon counter, Iqueye, mounted at the ESO 3.5 m New Technology Telescope. Thanks to the exquisite quality of the Iqueye data, we computed accurate phase coherent timing solutions for the two observing runs and over the entire year 2009. Our statistical uncertainty on the determination of the phase of the main pulse and the rotational period of the pulsar for short (a few days) time intervals are ≈1 μs and ∼0.5 ps, respectively. Comparison with the Jodrell Bank radio ephemerides shows that the optical pulse leads the radio one by ∼240 μs in January and ∼160 μs in December, in agreement with a number of other measurements performed after 1996. A third-order polynomial fit adequately describes the spin-down for the 2009 January plus December optical observations. The phase noise is consistent with being Gaussian distributed with a dispersion σ of ≈15 μs in most observations, in agreement with theoretical expectations for photon noise-induced phase variability.

Key words: pulsars: general – pulsars: individual: PSR B0531+21 (Crab nebula pulsar) – pulsars: individual: PSR J0534+2200 (Crab nebula pulsar).

1 INTRODUCTION

Only a handful of pulsars show optical emission at detectable levels and, among them, only five show pulsations in the optical band: the Crab (PSR B0531+21; PSR J0534+2200) and Vela (PSR B0833-45) pulsars, PSR B0540-69, PSR B0656+14, and Geminga (PSR B0630+17) (see e.g. Mignani 2011). The first source in which such pulsations were detected is the Crab nebula pulsar (Cocke, Disney & Taylor 1969; Lynds, Maran & Trumbo 1969). As such, the study of these pulsars, and in particular of the Crab which is the brightest among them ($V \sim 16.6$ mag), is of noticeable importance to understand the optical emission mechanism and to investigate, by comparison with the radio and other wavebands, the geometry of the emission regions and of the magnetic field.

The optical light curve of the Crab pulsar is well known. It is characterized by a double-peak folded profile, separated in phase by ∼0.4 (or ∼140°). It is very stable (Zampieri et al. 2011), although marginal evidence for a secular decrease in luminosity (Nasuti et al. 1996) and weak variations in the pulse shape (Karpov et al. 2007) have been reported.

Absolute optical timing of the Crab pulsar light curve has been addressed in some past investigations. For the other optical pulsars, with the sole exception of PSR B0540-69 (Middleditch, Pennypacker & Burns 1987; Gradari et al. 2011), the weakness of the targets prevented this type of studies till now. After the early attempts of Nelson et al. (1970), Papaliolios & Carleton (1970), and Horowitz et al. (1971), long-term (2 through 10 years) timing solutions for the Crab pulsar in the optical band were obtained by Boynton et al. (1972), Groth (1975a, 1975b), and Lohsen (1981), who found that the pulsar spin-down has a complex behaviour, including a secular slow-down accounted for (on average) by a cubic polynomial. Significant phase noise was observed in form of glitches, jumps, and random walks in frequency, but their origin remains as yet unknown. From an investigation of the radio timing of a sample of pulsars (not including the Crab), it has been proposed that often this behaviour may be induced by the abrupt change between two different spin-down rates resulting from variations in the pulsars magnetosphere (Lyne et al. 2010).

⋆ E-mail: luca.zampieri@oapd.inaf.it

© 2014 The Authors
Published by Oxford University Press on behalf of the Royal Astronomical Society

Downloaded from http://mnras.oxfordjournals.org/ at Uni Padova Fisica Astronomia on May 9, 2014

Recent investigations focused on the delay between the arrival time of the main pulse between the radio and other wavelengths, including the optical (e.g. Oosterbroek et al. 2006, 2008), and showed that the pulses in different energy bands are not aligned. This has profound implications for the geometry of the pulsar emission regions. All these studies have shown the relevance of independent timing studies in the optical (and other energy bands) to understand the pulsar emission mechanism by comparison with the radio. Our observations of the Crab pulsar with Iqueye are aimed at obtaining the most accurate optical timing needed to address these issues.

The plan of the paper is the following. Section 2 presents the Iqueye observations of the Crab pulsar and the adopted data reduction procedure. In Section 3, we show the phase fitting of the 2009 January and December data while, in Section 4, a comparison with the results from the radio ephemerides is presented. Section 5 is devoted to the phase coherent phase fit of the whole year 2009 data (some mathematical details are reported in Appendix A) and Section 6 to some conclusive remarks.

2 OBSERVATIONS AND DATA REDUCTION

The Crab nebula pulsar was observed with Iqueye mounted at the ESO 3.5 m New Technology Telescope (NTT) in two separate runs during 2009 January (from 15 through 20) and December (from 13 through 16). A log of the 20 observations performed in the two runs is reported in Table 1. All of them were done in white light. The average net count rate of the Crab pulsar during the observations was $\sim$4000 counts s^{-1}.

Iqueye is a very fast optical photon counter based on single photon avalanche photodiodes (SPAD) silicon detectors and equipped with a digital acquisition system that can record the photon arrival times of each single photon, similarly to what is usually done in High Energy and Space Astronomy. The relative/absolute timing accuracy is $\sim$0.2–0.6/1 ns for half-an-hour long observations. For a detailed description of the optomechanical design, data acquisition and control system, and data flow handling of the instrument, we refer to Naletto et al. (2009). After a split on a four-faced pyramid, Iqueye directs the incoming beam of light to four SPAD detectors. For the present analysis, their counts were summed together, so that the instrumental polarization coming from the four faces reflections was effectively averaged out. We considered also additional polarization-dependent effects possibly introduced by the reflection of the incoming light on the M3 mirror of NTT. However, no significant systematic variations (exceeding the statistical uncertainty) of the 2-s folded pulse profiles used for measuring the phase of the main peak (see Section 3) were noticed during hours long observations. We note that, in order to decrease the Crab nebula background and maximize the signal-to-noise ratio, during the 2009 observing runs Iqueye was operated with an entrance pinhole of 1.5″ radius, commensurate with the seeing conditions during the observations.

During the first observing night, we carefully checked for possible systematic frequencies in the data induced by telescope guiding and aperture loss effects. We did it by computing Fourier power spectra of several test targets. Apart from a low-frequency component caused by a digitization error of the azimuthal encoder of the telescope and promptly removed by the ESO staff, we found no spurious signals in the frequency range 1–2000 Hz. As a further check, a Fourier analysis of the Crab signal was performed for every observation and compared with that expected on the basis of the radio and our own ephemerides. Finally, we simulated also the system behaviour assuming small periodic intensity variations of the signal caused by telescope guide, wind shaking and similar effects, which could be amplified by the rather tight match between pinhole size and seeing. We then estimated the high-frequency noise possibly induced by a sinusoidal intensity noise of small amplitude ($<$10 per cent of the average pulsar signal) and found that it has negligible effects ($<$ a few μs) on the determination of the peak arrival time for sampling frequencies below a few Hz (which includes our adopted light curve sampling time of 2 s; see Section 3). However, this additional phase noise may explain the excess width of the distribution of residuals that we noticed in some observations (see Section 5).

The data reduction procedure consists of converting the arrival time tags of each photon in local UTC time by means of our own developed software (QUEST v. 1.1.1; P. Zoccarato, internal technical

Table 1. Log of the 2009 observations of the Crab nebula pulsar, taken with Iqueye mounted at the ESO 3.5 m NTT telescope in Chile. Times refer to the barycentre of the Solar system (TEMPO1).

	Observation ID	Start time (UTC)	Start time (MJD)	Duration (s)
1	20090115-030226UTC_crab2	January 15, 03:11:14.9	548 46.132 811	255.2
2	20090115-031933UTC_crab3	January 15, 03:28:07.8	548 46.144 535	198.2
3	20090115-032345UTC_crab4	January 15, 03:32:18.8	548 46.147 440	897.8
4	20090116-014452UTC_crab	January 16, 01:53:40.9	548 47.078 946	156.9
5	20090116-014802UTC_crab	January 16, 01:56:48.7	548 47.081 119	98.2
6	20090116-015011UTC_crab	January 16, 01:59:10.9	548 47.082 765	233.7
7	20090116-015448UTC_crab2	January 16, 02:03:37.6	548 47.085 852	1997.6
8	20090117-012137UTC_crab	January 17, 01:30:18.3	548 48.062 712	3597.5
9	20090118-014557UTC_crab	January 18, 01:55:02.2	548 49.079 887	727.1
10	20090118-020018UTC_crab	January 18, 02:09:22.3	548 49.089 842	5997.2
11	20090119-004736UTC_crab	January 19, 00:56:09.6	548 50.039 000	3598.1
12	20090120-012735UTC_crab	January 20, 01:36:16.4	548 51.066 857	3712.7
13	20091213-034209UTC_crab-NTT	December 13, 03:51:47.5	551 78.160 966	178.3
14	20091213-035043UTC_crab-NTT	December 13, 04:00:33.5	551 78.167 054	1798.2
15	20091213-042211UTC_crab-NTT	December 13, 04:31:47.5	551 78.188 744	6.1
16	20091214-023608UTC_crab-NTT	December 14, 02:46:08.7	551 79.115 379	7198.2
17	20091214-043954UTC_crab-NTT	December 14, 04:49:32.8	551 79.201 074	7198.3
18	20091215-031945UTC_crab-NTT	December 15, 03:29:34.9	551 80.145 543	7198.6
19	20091216-021802UTC_crab-NTT	December 16, 02:27:33.9	551 81.102 476	3598.5
20	20091216-031834UTC_crab-NTT	December 16, 03:28:05.9	551 81.144 513	898.3

Downloaded from http://mnras.oxfordjournals.org/ at Uni Padova Fisica Astronomia on May 9, 2014

Table 2. Geocentric coordinates of the ESO 3.5 m NTT telescope in La Silla. The 3σ uncertainty is 0.3 m.

x (m)	y (m)	z (m)
1838 193.8	−5258 983.6	−3100 153.5

report). Times are then referred to the Solar system barycentre using the software TEMPO2[1] (Hobbs, Edwards & Manchester 2006; Edwards, Hobbs & Manchester 2006). For the sake of comparison with the Jodrell Bank monthly ephemerides (Lyne, Pritchard & Graham-Smith 1993),[2] we decided to use TEMPO2 in TEMPO1 emulation mode and to adopt the same position for the Crab pulsar (RA $05^{h}34^{m}31^{s}.972\ 32$, Dec. $+22^{\circ}00'52''.0690$ [J2000]), with no correction for proper motion. To perform barycentric corrections, the software also needs an accurate value of the observatory geocentric coordinates (Table 2). They were measured with a GPS receiver connected to an antenna situated at the dome of the telescope. The final position was referred to the intersection of the telescope azimuth and elevation axes by laser assisted metrology.

3 PHASE FITTING 2009 JANUARY AND DECEMBER RUNS

Each barycentric corrected time series is divided in short segments 2 s long and folded over a reference period $P_{\rm init}$. In order to cross check the accuracy of our results, in each segment the phase of the main pulse is determined using two different methods: (a) calculating the maximum of the cross-correlation function between the 2-s folded profile and a smoothed pulse shape of the whole data set (see Germanà et al. 2012). The latter is a numerical template, obtained by smoothing the distribution generated by the counts of all observations distributed according to their phase of arrival; (b) fitting the main peak and the interpulse in the 2-s folded profile with an analytic template, constructed to provide an accurate representation of the smoothed pulse shape of the whole data set (sum of Lorentzians; see Fig. 1 and Table 3). The fitting parameters are the total amplitude p, the background level q, and the centroid of the first Lorentzian x_1.[3] The adopted phase bin is 1/300 in method (a) and 1/1000 in method (b). The two algorithms return phase measurements that are in agreement within the errors. The typical spread in phase measurements for 2-s long segments is ∼0.005 in phase, or ∼17–18 μs in time.

Phase measurements of the main peak track pulsar spin-down with respect to uniform rotation. If ϕ is the phase of the pulsar main peak and $\phi' = \nu_{\rm init}(t - t_0)$ the phase of a uniform rotator with frequency $\nu_{\rm init} = 1/P_{\rm init}$, the actual measured phase is

$$\psi(t) = \phi(t) - \phi'(t) = \phi(t) - \frac{1}{P_{\rm init}}(t - t_0)\,, \qquad (1)$$

where t_0 is the time (the starting Julian date of the observing run) at which ϕ and ψ agree up to an integer number of ϕ turns. ψ represents the difference between the phase of the pulsar and that

[1] http://www.atnf.csiro.au/research/pulsar/ppta/tempo2

[2] http://www.jb.man.ac.uk/∼pulsar/crab.html

[3] The peak of the analytic template is at $x_{\rm max} = x_1 - 9.6 \times 10^{-5}$. However, the phase of the main pulse in each segment is taken to be $x_p = x_1 + 1.2 \times 10^{-5}$, where the shift ($1.2 \times 10^{-5}$) is inferred from fitting the smoothed pulse shape with the analytic template itself.

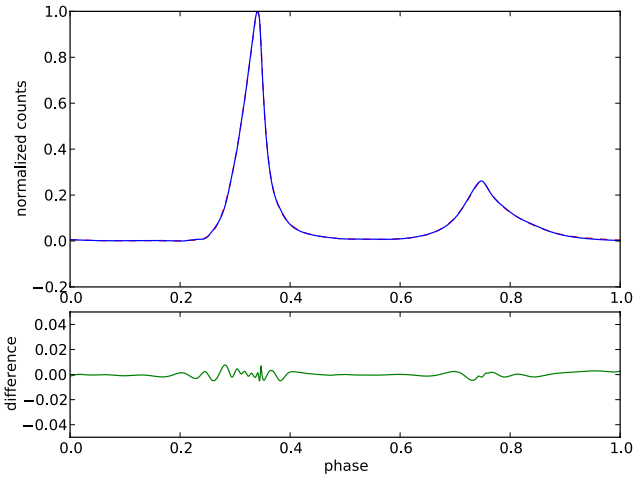

Figure 1. Upper panel: analytic template (solid line) adopted to fit the Crab pulse shape (method b in the text), obtained from the sum of 16 Lorentzians. The smoothed pulse shape of the whole data set (see text for details) is beneath the solid one. The two curves are normalized to the maximum of the smoothed pulse shape. The difference between the two curves is shown in the bottom panel. The interval adopted to perform the fit is between −0.07 and 0.54 from the position of the main peak. In this interval, the difference is at most ≃0.006 on the tails of the peaks (where the normalized counts ∼0.1), which corresponds to a fractional difference ≃6 per cent.

of the uniform rotator and its fractional part is determined by cross-correlating or fitting the measured pulse shape as described above. The integer part is found as explained below.

Since the pulsar frequency changes only slowly in time, the phase ψ is modelled with a timing solution in the form of a second-order polynomial:

$$\psi(t) = \phi_0 + (\nu_0 - \nu_{\rm init})(t - t_0) + \frac{1}{2}\dot{\nu}_0(t - t_0)^2\,, \qquad (2)$$

where ϕ_0, ν_0, $\dot{\nu}_0$ are the actual pulsar phase, rotational frequency, and its first derivative at t_0, respectively. The reference time is $t_0^{\rm J} = 548\,46$ MJD for January and $t_0^{\rm D} = 551\,78$ MJD for December. On intervals of a few days, this expression is statistically adequate to describe the phase behaviour. On longer time intervals, higher order terms become important (see Section 5).

Fig. 2 shows the timing solutions for 2009 January and December obtained fitting equation (2) to the measured phases by means of a χ^2 minimization procedure. The adopted reference periods $P_{\rm init}$ are 0.033 625 270 5350 s and 0.033 637 181 7073 s, respectively, and the reference epochs are those given in Table 4. Since the correlation/fitting procedure can only give the fractional part of the phase, the integer part of the phase difference between successive nights are found by minimizing χ^2 with respect to integer variations of ψ. The best-fitting parameters are reported in Table 4, along with the arrival time of the main peak after mid-night $t_{\rm arr} = \phi_0 P_{\rm init}$ and the pulsar rotational period $P_0 = 1/\nu_0$ at t_0. Quoted errors are purely statistical and correspond to the 2σ confidence level for one interesting parameter.

4 COMPARISON WITH JODRELL BANK RADIO EPHEMERIDES: OPTICAL-RADIO PHASES

We can compare rotational phases and arrival times of the main peak in the optical with phases and arrival times in the radio, reported in the Jodrell Bank Crab Pulsar Monthly Ephemeris website

Downloaded from http://mnras.oxfordjournals.org/ at Uni Padova Fisica Astronomia on May 9, 2014

Table 3. Analytic template (16 Lorentzians) adopted to fit the Crab pulse shape (p, q, x_1 free parameters): $f(x) = p\sum_{i=1}^{16} d_{i-1}b_i^2/[b_i^2 + (x - x_1 + h_{i-1})^2] + q$.

Parameter	Value	Parameter	Value	Parameter	Value
b_1	0.014 6996	d_0	1	h_0	0
b_2	0.014 6996	d_1	0.217 538	h_1	0.029 5389
b_3	0.014 6996	d_2	0.120 438	h_2	0.045 2724
b_4	0.014 6996	d_3	0.343 795	h_3	0.015 9706
b_5	0.014 6996	d_4	0.027 4555	h_4	−0.040 5742
b_6	0.003 906 05	d_5	0.104 503	h_5	−0.004 064
b_7	0.013 1649	d_6	0.052 4991	h_6	−0.408 426
b_8	0.051 7911	d_7	0.046 2601	h_7	−0.493 455
b_9	0.038 6609	d_8	0.250 336	h_8	−0.400 741
b_{10}	0.037 7745	d_9	0.063 293	h_9	−0.445 372
b_{11}	0.015 6592	d_{10}	−0.032 3015	h_{10}	0.094 8912
b_{12}	0.032 5165	d_{11}	−0.017 6647	h_{11}	0.133 417
b_{13}	0.053 1056	d_{12}	0.012 8576	h_{12}	0.355 586
b_{14}	0.209 385	d_{13}	0.009 443 15	h_{13}	−0.020 0141
b_{15}	−0.063 0249	d_{14}	−0.008 832 56	h_{14}	−0.261 205
b_{16}	0.025 9154	d_{15}	−0.003 886 52	h_{15}	−0.153 419

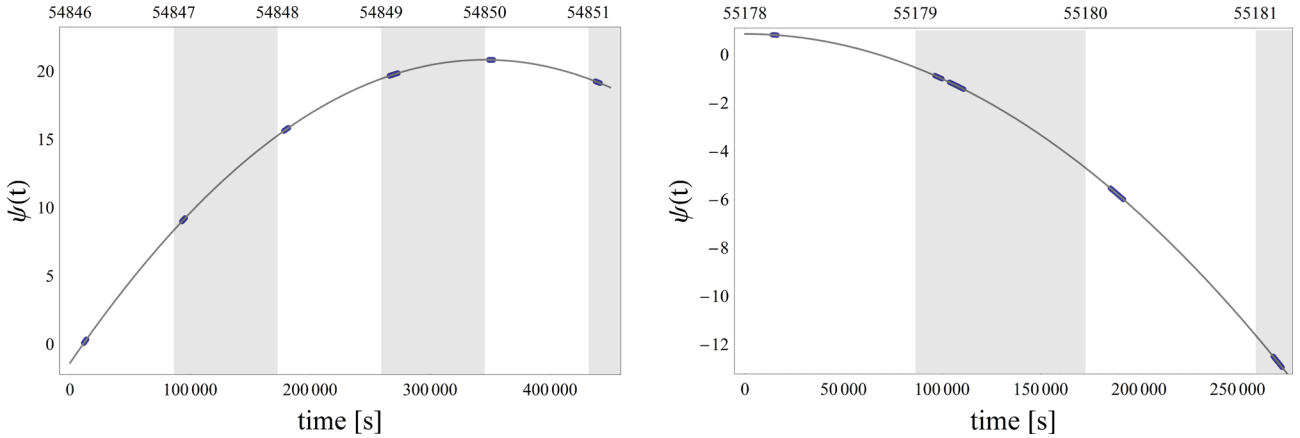

Figure 2. Phase ψ of the Crab pulsar (with respect to uniform rotation) during the January (left) and December (right) Iqueye runs. Time on the top axis is expressed in Modified Julian Date (MJD). The timing solution does not include the cubic term.

Table 4. Timing solutions for the two separate 2009 January and December data sets.

	2009 January observations[a]
t_0 (MJD)	548 46.0
ϕ_0	$0.632\,498 \pm 5.0 \times 10^{-5}$
ν_0 (s^{-1})	$29.739\,666\,163\,27 \pm 4.4 \times 10^{-10}$
$\dot{\nu}_0$ (s^{-2})	$-3.717\,790 \times 10^{-10} \pm 1.7 \times 10^{-15}$
P_0 (s)	$0.033\,625\,125\,2623 \pm 5.0 \times 10^{-13}$
t_{arr} (s)[b]	$0.021\,2678 \pm 1.7 \times 10^{-6}$
	2009 December observations[c]
t_0 (MJD)	551 78.0
ϕ_0	$0.853\,410 \pm 3.6 \times 10^{-5}$
ν_0 (s^{-1})	$29.729\,006\,688\,22 \pm 5.2 \times 10^{-10}$
$\dot{\nu}_0$ (s^{-2})	$-3.714\,336 \times 10^{-10} \pm 3.2 \times 10^{-15}$
P_0 (s)	$0.033\,637\,181\,7090 \pm 5.8 \times 10^{-13}$
t_{arr} (s)[b]	$0.028\,7063 \pm 1.2 \times 10^{-6}$

[a] $P_{init} = 0.033\,625\,270\,5350$ s.
[b] Arrival time of the main peak after t_0: $t_{arr} = \phi_0 P_{init}$.
[c] $P_{init} = 0.033\,637\,181\,7073$ s.

(JB ephemerides hereafter; Lyne et al. 1993, see footnote 2). Radio phases are calculated using equation (2), where the values of $\phi_{0,r}$, $\nu_{0,r}$, $\dot{\nu}_{0,r}$ are computed from the closest available epoch reported in the JB archive (usually day 15 of each month).

Fig. 3 shows the difference between the optical and radio timing solutions. The residuals and optical–radio phase difference are computed from the global fit of all the 2009 Iqueye observations (see Section 5). Considering only the statistical error on the optical data, the average difference between the time of arrival of the optical and radio peaks is ∼240 μs in 2009 January and ∼160 μs in December. The total uncertainties (statistical plus systematics) on JB radio ephemerides is 90 μs in January and 200 μs in December. Therefore, the optical–radio difference is significant only for January data, with the optical peak leading the radio one. An independent measurement of the 2009 December optical–radio phase shift (∼178 μs), based on the same Iqueye data, was obtained by Collins et al. (2012) using simultaneous JB radio observations and is consistent with that reported here.

In addition to the optical–radio phase difference, Fig. 3 also indicates the existence of a phase drift. Considering the optical–radio phase difference from the fit of each observing run separately, they amount to 3.7±0.1 and 17.5±0.2 μs d^{-1} for January and December, respectively.

Downloaded from http://mnras.oxfordjournals.org/ at Uni Padova Fisica Astronomia on May 9, 2014

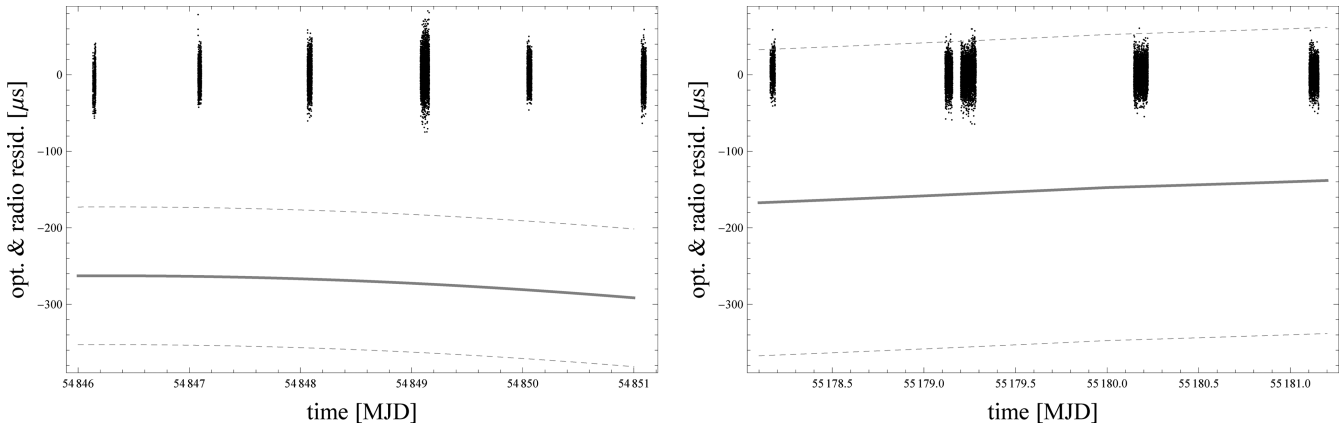

Figure 3. Phase residuals for the January (left) and December (right) Iqueye runs. The solid line represents the difference between the optical and radio timing solutions, while the dashed lines bound the total (statistical plus systematic) uncertainty on the radio phases. The residuals and optical–radio phase difference are computed from the global fit of all the 2009 Iqueye observations (see Section 5).

5 PHASE-COHERENT OPTICAL TIMING SOLUTION IN 2009

The quality of the Iqueye data is such that we can attempt to connect the phases measured several months apart in the optical band, if we assume that the pulsar is slowing down quite regularly according to a simple braking law. We recomputed the phases for all the 2009 observations reported in Table 1 following the approach outlined in Section 3 and taking as common reference period for the two runs $P_{\rm init} = 0.033\,625\,130\,000\,00$ s. For the sake of comparison with the 'local' January and December timing solutions, two different reference epochs are adopted, MJD 548 46 and 551 78 (see below).

On a 1 yr time interval, the parabolic spin-down model of equation (2) is no longer adequate to describe the behaviour of the phases. We then adopted a cubic polynomial of the form (e.g. Boynton et al. 1972):

$$\psi(t) = \phi_0 + (\nu_0 - \nu_{\rm init})(t - t_0) + \frac{1}{2}\dot{\nu}_0(t - t_0)^2 + \frac{1}{6}\ddot{\nu}_0(t - t_0)^3, \tag{3}$$

where $\ddot{\nu}_0$ is the second derivative of the rotational frequency at t_0. In several spin-down models, the pulsar frequency derivative $\dot{\nu}$ is predicted to satisfy the well-known braking index relation:

$$\dot{\nu} = -K\nu^n, \tag{4}$$

where K is a constant and n, the braking index, depends on the physical mechanism responsible for the loss of angular momentum and rotational energy of the star. Using this expression and adding the fourth-order term, equation (3) can be cast in the form

$$\psi(t) = \phi_0 + (\nu_0 - \nu_{\rm init})(t - t_0) + \frac{1}{2}\dot{\nu}_0(t - t_0)^2 + \frac{n}{6}\frac{\dot{\nu}_0^2}{\nu_0}(t - t_0)^3 + \frac{n(2n-1)}{24}\frac{\dot{\nu}_0^3}{\nu_0^2}(t - t_0)^4. \tag{5}$$

We can estimate the importance of the parabolic, cubic and fourth-order terms in the Taylor expansion (5). The spin-down is sensitive to them if they contribute at least a significant number of rotations, say $\Delta\psi \approx 10$. Assuming $\nu_0 \approx 30$ Hz and $\dot{\nu}_0 \approx -4 \times 10^{-10}$ s^{-2}, this requires a time $\Delta t_2 = |2\Delta\psi/\dot{\nu}_0|^{1/2} \approx 2.5$ d for the parabolic term, $\Delta t_3 = (6\Delta\psi\nu_0/(n\dot{\nu}_0^2))^{1/3} \approx 180$ d for the cubic term, and $\Delta t_4 = |24\Delta\psi\nu_0^2/((2n^2 - n)\dot{\nu}_0^3)|^{1/4} \approx 4$ yr for the fourth-order term to become important. Therefore, while it is meaningful to adopt equation (2) for a single observing run, a full timing solution over 1 yr requires a cubic spin-down representation as in equation (3) (e.g. Boynton et al. 1972). Higher order terms are needed for longer time intervals.

Table 5. Timing solutions for whole year 2009. Two solutions are reported, corresponding to two different reference epochs (MJD 548 46 and 551 78, respectively.

	All 2009 Iqueye observations[a]
$\hat{t}_0$ (MJD)	548 46
ϕ_0	$0.632\,777 \pm 3.2 \times 10^{-5}$
ν_0 (s^{-1})	$29.739\,666\,160\,36 \pm 1.1 \times 10^{-10}$
$\dot{\nu}_0$ (s^{-2})	$-3.717\,692\,75 \times 10^{-10} \pm 1.8 \times 10^{-17}$
$\ddot{\nu}_0$ (s^{-3})	$1.131\,83 \times 10^{-20} \pm 1.2 \times 10^{-24}$
P_0 (s)	$0.033\,625\,125\,265\,62 \pm 1.2 \times 10^{-13}$
$t_{\rm arr}$ (s)[b]	$0.021\,2772 \pm 1.1 \times 10^{-6}$
n[c]	$2.435\,39 \pm 0.000\,26$
$\hat{t}_0$ (MJD)	551 78
ϕ_0	$0.853\,283 \pm 2.2 \times 10^{-5}$
ν_0 (s^{-1})	$29.729\,006\,689\,51 \pm 1.3 \times 10^{-10}$
$\dot{\nu}_0$ (s^{-2})	$-3.714\,446\,13 \times 10^{-10} \pm 1.9 \times 10^{-17}$
$\ddot{\nu}_0$ (s^{-3})	$1.131\,83 \times 10^{-20} \pm 1.2 \times 10^{-24}$
P_0 (s)	$0.033\,637\,181\,707\,55 \pm 1.4 \times 10^{-13}$
$t_{\rm arr}$ (s)[b]	$0.028\,691\,75 \pm 7.4 \times 10^{-7}$
n[c]	$2.438\,78 \pm 0.000\,26$

[a] $\hat{P}_{\rm init} = 0.033\,625\,130\,000\,00$ s, $\Delta\hat{\psi}_n = 152\,784$, $N = 852\,923\,471$.
[b] Arrival time of the main peak after t_0: $t_{\rm arr} = \phi_0 P_{\rm init}$.
[c] Braking index: $n = -\nu_0\ddot{\nu}_0/\dot{\nu}_0^2$.

The phase fit with the cubic spin-down model of equation (3) of all the 2009 (January and December) optical phase measurements has been performed in two different ways. In the first approach, the pulsar phases determined in Section 3 (ψ phases) are directly fitted adding a phase shift to the December data set as described below. In the second approach, the true pulsar rotational phases (ϕ phases) are reconstructed for each observing run and the fit is performed after determining the integer phase shift between January and December, as explained below. The two approaches return results in agreement within 3σ. They are shown in Table 5. For the sake of comparison with the 'local' January and December timing solutions, in the first approach two independent fits of the whole data set are performed, assuming as reference epochs MJD 548 46 or 551 78, respectively.

Downloaded from http://mnras.oxfordjournals.org/ at Uni Padova Fisica Astronomia on May 9, 2014

The quoted errors are purely statistical and correspond to the 2σ confidence level for one interesting parameter.

To perform the fit using the first approach, the two data sets of January and December had to be referred to a common reference period $\hat{P}_{\rm init}$. Phase folding becomes inaccurate if there is a significant mismatch between $\hat{P}_{\rm init}$ and the actual pulsar period, which is different in January and December. Therefore, phases were first computed using the reference periods reported in Table 4 and then referred to $\hat{P}_{\rm init}$ for both the January and December data using the two expressions (see Appendix A):

$$\hat{\psi}_{\rm J}(t) = u\,fr[\psi_{\rm J}(t)] - (u-1)\,n(t) - v - \hat{\psi}_{n,{\rm J}} \quad (6)$$

$$\hat{\psi}_{\rm D}(t) = u\,fr[\psi_{\rm D}(t)] - (u-1)\,n(t) - v - \hat{\psi}_{n,{\rm D}} - \Delta\hat{\psi}_n, \quad (7)$$

where $u = P^{\rm J,D}_{\rm init}/\hat{P}_{\rm init}$, $n(t) = {\rm int}[(t_{\rm p} - t_0^{\rm J,D})/P^{\rm J,D}_{\rm init}] = {\rm int}[(t - t_0^{\rm J,D})/P^{\rm J,D}_{\rm init}]$,[4] $v = fr[(t_0^{\rm J,D} - \hat{t}_0)/\hat{P}_{\rm init}]$ and $fr[\,]$ denotes the fractional part. Equations (6) and (7) come from the requirement that the time of arrival of a single pulse determined in the two different 'temporal gauges' be equal (or, similarly, that the phase ϕ of the main pulse computed using ψ or $\hat{\psi}$ be equal; see Appendix A). We adopted $\hat{P}_{\rm init} = 0.033\,625\,130\,000\,00$ s (Table 5). The phase shifts $\hat{\psi}_{n,{\rm J}}$ and $\hat{\psi}_{n,{\rm D}}$ are the integer part of the phase difference between successive nights in January and December, respectively, and are found by minimizing χ^2 with respect to integer variations of $\hat{\psi}$, as explained in Section 3. An additional integer shift $\Delta\hat{\psi}_n$ is needed to phase connect together the January and December data sets and is also determined through χ^2 minimization.

In the second approach, we express the phase ϕ using equation (1) for both the January and December data as

$$\phi_{\rm J}(t) = \psi_{\rm J}(t) + \frac{1}{P^{\rm J}_{\rm init}}\left(t - t_0^{\rm J}\right) \quad (8)$$

$$\phi_{\rm D}(t) = \psi_{\rm D}(t) + \frac{1}{P^{\rm D}_{\rm init}}\left(t - t_0^{\rm D}\right) + N, \quad (9)$$

where N is an integer phase shift. The union of the two sets of data is fitted to a cubic polynomial with the unknown integer N as a fitting parameter, which is varied to produce the minimum value of χ^2.

Up to third order, the braking index model (equation 5) is essentially indistinguishable from the cubic spin-down model, both having four free parameters. In fact, the pulsar braking index can be determined directly fitting equation (5), truncated to third order, to the data or from the pulsar frequency and its first and second derivatives: $n = -\nu_0\ddot{\nu}_0/\dot{\nu}_0^2$. The measured value is again reported in Table 5.

A phase coherent timing solution for year 2009 can also be derived from the JB radio ephemerides. The calculation is performed in a similar way, fitting equation (3) to the phases reported in the JB archive. The values of radio phase, frequency and its derivatives are usually given at day 15 of each month. They are computed as averages of different measurements performed during the month. From $\phi_{0,r}$, $\nu_{0,r}$, $\dot{\nu}_{0,r}$ at day 15, we extrapolate the phases from $\sim$15 d before through $\sim$15 d after the epoch reported in the ephemerides and match them at the beginning of each month. This is done using equation (3) and approximating $\ddot{\nu}_{0,r} \approx 2\nu^3_{0,r}\,\dot{\nu}^2_{0,r}$, as suggested in the explanatory set of notes of the JB ephemerides (see footnote 2). The matching precision at monthly intervals is consistent with the uncertainty reported in the JB archive ($\sim$100–200 μs). A single cubic global fit of the radio phases is then performed with equation (3).

[4] $t_{\rm p}(t)$ is the time of arrival of the main pulse after time t.

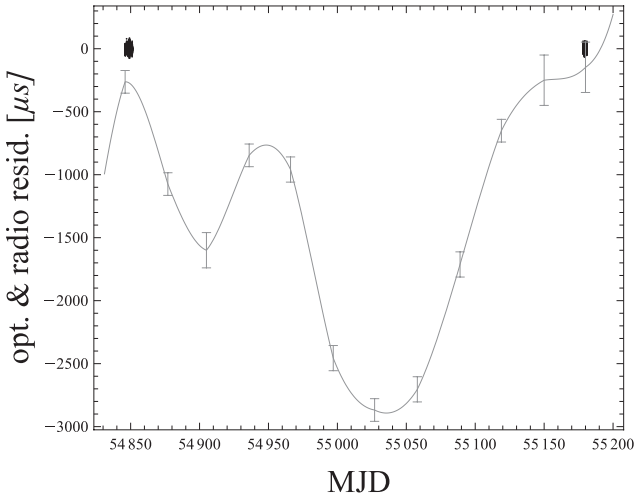

Figure 4. Phase residuals for all the 2009 Iqueye observations (black dots) and the JB ephemerides (grey vertical bars) with respect to the optical fit with the cubic spin-down model reported in Table 5 ($\Delta\hat{\psi}_n = 152\,784$, $N = 852\,923\,471$). The grey solid line represents a smooth curve joining the average monthly cubic fits of the JB ephemerides. The vertical error bars are the total (statistical plus systematic) uncertainty on the radio phases as quoted in JB ephemerides.

The χ^2 of the fit is 345 for 12 degrees of freedom, which tells that the assumption of a constant braking law is not valid. Excursions of the radio phases about the cubic fit from the optical data, shown in Fig. 4, are larger than measurement uncertainties.

The short-term (monthly) radio phase behaviour differs from the one predicted by equations (3) or (5) because of the effects of pulsar rotational variations and irregularities that build up on the radio monthly time-scale, but are not visible on the coarser year-time-scale of our optical observations. However, on average the cubic fit appears to account quite nicely for the long-term phase evolution of the pulsar rotation (see e.g. Groth 1975b). With the choice of $\Delta\hat{\psi}_n$ and N described below, the residual timing difference between the radio and optical cubic fits is only a few ms (with small differences also in the frequency, its derivatives, and braking indices). This deviation is at most $\sim$0.1 turns, which amounts to $\sim 10^{-10}$ parts of the phase increment on the time interval sampled by observations. We conclude that the pulsar phase follows the constant braking law quite closely, yet not absolutely precisely.

We also note that the braking index inferred from the radio data differs from that obtained in previous epochs. Taking as reference MJD 550 00, close to the middle of the interval, $n_{\rm radio} = 2.4585 \pm 0.0022$. This is smaller than the average value measured in the radio during years 1969 through 1993 ($n_{\rm radio} = 2.51 \pm 0.01$; Lyne, Pritchard & Graham-Smith 1988; Lyne et al. 1993), indicating a change in the strength of the spin-down.

Using the two approaches described above, the integer phase shifts needed to phase connect the December to the January Iqueye data are determined through χ^2 minimization. Four adjacent values of N give a χ^2 which lies in the interval of 90 per cent statistical significance of the χ^2 distribution for 22 525 independent variables (the number of phases measured). They are: 852 923 566, 852 923 567 (absolute minimum), 852 923 568, 852 923 569. We consider all these four fits acceptable. Similarly, four values of $\Delta\hat{\psi}_n$ lie in the 90 per cent interval of the χ^2 distribution of the fit: 152 784, 152 785, 152 786 (absolute minimum), 152 787. As discussed above, because of our limited temporal sampling, we were not in a position to detect

Downloaded from http://mnras.oxfordjournals.org/ at Uni Padova Fisica Astronomia on May 9, 2014

monthly phase oscillations that the pulsar made during 2009. Therefore, just from optical data we could not decide between the four different values of N or $\Delta\hat{\psi}_n$. Tracking the long-term behaviour with a finer temporal coverage, the radio data allow us to single out the values of $\Delta\hat{\psi}_n$ (152 784) and N (852 923 469) which have been used to construct the optical fit shown in Fig. 4. Using these values, the number of pulsar turns between MJD 548 46 and 551 78 is in agreement with the value calculated from the JB ephemerides. We obtain $N_\phi = \mathrm{int}[\phi_\mathrm{D}(t_0^\mathrm{D}) - \phi_\mathrm{J}(t_0^\mathrm{J})] = 852\,923\,571$ from equations (8) and (9), and $N_{\hat{\psi}} = \mathrm{int}[\hat{\psi}(t_0^\mathrm{D}) - \hat{\psi}(t_0^\mathrm{J}) + (t_0^\mathrm{D} - t_0^\mathrm{J})/\hat{P}_\mathrm{init}] = 852\,923\,571$ from equations (1), (6) and (7).

We note that the uncertainties of the parameters quoted in Table 5 are strictly formal statistical 2σ confidence intervals, calculated with the assumption that a single N or $\Delta\hat{\psi}_n$ (the one which corresponds to the absolute minimum of the χ^2) is the correct solution of the problem. As discussed above, the comparison of radio and optical data reveals that the constant braking law assumption is a good, but not exact, approximation of the pulsar's phase development. Taking this into account, the errors in Table 5 should be revised considering the range of values of the parameters obtained from all the fits that we consider acceptable. They are of the order of 10^{-4} for ϕ_0, 10^{-9} s^{-1} for ν_0, 10^{-14} s^{-2} for $\dot{\nu}_0$, 10^{-21} s^{-3} for $\ddot{\nu}_0$, 10^{-1} for n, 10^{-12} s for P, 10^{-5} s for t_arr. The errors inferred from the fits of the January and December runs separately (Table 4) are more representative of the actual uncertainty for short (a few days) time intervals.

A consequence of the intrinsic irregularities of the pulsar rotation can be seen comparing the values of ϕ_0, ν_0, and $\dot{\nu}_0$ obtained from the 'local' parabolic fits (Table 4) and the global 2009 cubic fit (Table 5). The differences in some of the fitted parameters (e.g. ϕ_0 and ν_0 in December) are larger than the uncertainty. This shows that a few observing nights are sufficient to reduce the statistical error to the point that we become sensitive to effects related to the long-term phase noise of the pulsar (see Section 6). Despite these differences, the optical-radio phase shift observed in January and December is robustly recovered from both the 'local' and global timing solutions, indicating that it is not an effect of radio data long-term averaging.

We studied also the distribution of the phase residuals about their best-fitting polynomials. The residuals are computed with respect to the timing solution reported in Table 5 (solution for $t_0 = 548\,46$). The optical phase residuals can be satisfactorily fitted with a Gaussian with a dispersion σ between 15 and 22 μs (see Fig. 5). The Gaussian distribution provides a good fit of residuals of single observing nights, as well as of residuals with respect to the 2009 coherent timing solution, with a $\sigma = 17.3$ μs, which is essentially the average value of single night residuals.

The width of the distribution is consistent with that induced by pure photon counting noise, as simulated using a synthetic signal that has the same pulse shape, average count rate, and background level of the Crab pulsar observed with Iqueye at NTT. We note that different observations have slightly different widths, most likely because of the different quality of the sky during the various nights, as discussed in Section 2.

6 DISCUSSION AND CONCLUSIONS

The measurement of the optical–radio phase shift, obtained with Iqueye in 2009 (∼240 μs in January; ∼160 μs in December), is consistent with that determined in our previous measurement performed with Aqueye in Asiago in 2008 October (∼230 μs; Germanà et al. 2012). The optical pulse always leads the radio one. This is also in agreement with a number of other measurements performed after 1996 (see e.g. Oosterbroek et al. 2008). Only a couple of previous measurements yielded different results (consistent with no or negative delay; Golden et al. 2000; Romani et al. 2001), possibly because some systematics were not adequately accounted for (e.g. the difference between the phase of the peak of the main pulse and the phase of the centroid of the main pulse, which is due to the asymmetric pulse shape). Therefore, although it is not possible to exclude a secular change of the phase delay, the available data show that the pulse in the optical leads that in the radio by 150–250 μs (see also Strader et al. 2013). This can be caused by a different position of the two emitting regions (50–80 km), although this is difficult to understand as electrons close to the pulsar are highly relativistic and any travel time delay between electrons and photons is essentially negligible. Most probably, the optical and radio beams are misaligned (1.5°–3°) because at the position where electrons emit optical photons the magnetic field has a slightly different orientation with respect to that where radio emission takes place.

The counting statistics available in the optical band allows us to compute the timing solution with extreme accuracy from a small number of consecutive observing nights, with an error of only $\approx 3 \times 10^{-5}$ in fractional phase or ≈1 μs in time (see Table 4). The optical timing solution matches the radio phase quite closely, yet in addition to a presumably constant phase shift between optical and radio, we find small ≈10 μs d^{-1} phase drifts between the two solutions, which are consistent with timing noise deduced from radio and optical data and with residuals effects of changing dispersion measures on the radio data.

The distributions of phase residuals are well approximated by Gaussians. The best observations have a dispersion $\sigma \approx 15$ μs (with 2 se sampling), in agreement with theoretical expectations for pure photon noise-induced phase variability. However, a few January and December observations have a slightly larger spread (≈20 μs), which is most likely caused by worse quality of the sky. We note that the dispersion of residuals in our data is much smaller than the dispersion of the residuals for Giant Radio Pulses (84 μs) recently reported by Bhat, Tingay & Knight (2008).

Giving the exquisite precision of the Iqueye data, we were able to phase connect the January and December observing runs, obtaining a global third-order timing solution for year 2009 and an independent measurement of the pulsar braking index. A comparison with the 2009 timing solution in the radio band shows that the pulsar makes small amplitude random excursions/oscillations around the 'average' cubic spin-down (with residuals up to a few ms in phase and a jitter up to $\sim 10^{-8}$ Hz in frequency), that are statistically significant. Imposing that the number of optical turns be equal to that in the radio band, the optical, and radio phases in January and December are very close, but at intermediate times phase predictions differ. As a consequence, the inferred values of the frequency, its derivatives, and braking indices also differ. Therefore, while the third-order secular spin-down and braking index model are very good at reproducing the overall evolution of the phases (e.g. Groth 1975b), an accurate description of the pulsar phase excursions/oscillations requires a frequent monitoring on a monthly time-scale.

The optical observations reported here confirm the third-order secular spin-down and braking index model to a high degree of accuracy. During the period from 2009 January to December, the pulsar has followed a braking index law so closely that, from the two Iqueye sets of observations alone, we were able to count the almost nine hundred million turns that the pulsar has made with an uncertainty of only two turns.

Future and more regular observations taken with both Iqueye and its twin Aqueye, mounted at the Copernico telescope in Asiago, will

Downloaded from http://mnras.oxfordjournals.org/ at Uni Padova Fisica Astronomia on May 9, 2014

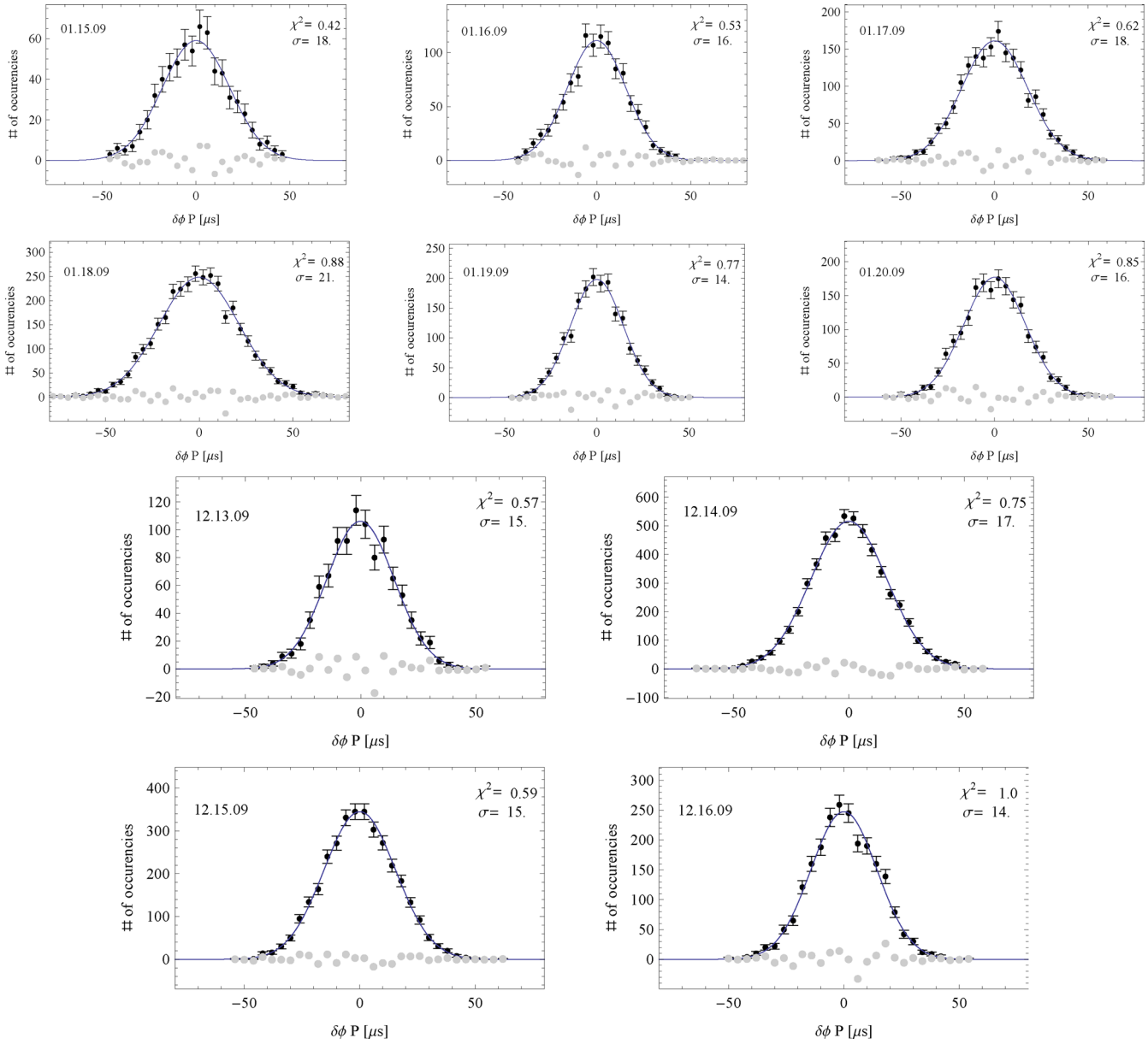

Figure 5. Distribution of phase residuals for the various 2009 Iqueye observing nights. Data are binned with 32 bins of 2.5 μs each. The solid line is the Gaussian fit, while the grey dots without error bars represent the difference between the data and the fit. The reduced χ^2 of the fit and the dispersion σ of each Gaussian (in μs) are also shown. From *top-left* to *bottom-right*: January 15, 16, 17, 18, 19, 20; December 13, 14, 15, 16.

offer an invaluable means to monitor the optical–radio phase delay, to understand the phase excursions around the braking index model and to pinpoint the deep physical origin of the pulsar spin-down mechanism.

ACKNOWLEDGEMENTS

We thank the referee for their report with helpful comments that improved the paper, Claudio Germanà for useful discussions, and Ivan Capraro, Andrea Di Paola and Claudia Facchinetti for their contribution to the realization of Iqueye. This work is based on observations made with ESO Telescopes at the La Silla Paranal Observatory under programme IDs 082.D-0382 and 084.D-0328(A). We acknowledge the use of the Crab pulsar radio ephemerides available at the website of the Jodrell Bank radio Observatory (http://www.jb.man.ac.uk/~pulsar/crab.html; Lyne et al. 1993). This research has been partly supported by the University of Padova under the Quantum Future Strategic Project, by the Italian Ministry of University MIUR through the programme PRIN 2006 and by the Project of Excellence 2006 Fondazione CARIPARO.

REFERENCES

Bhat N. D. R., Tingay S. J., Knight H. S., 2008, ApJ, 676, 1200
Boynton P. E., Groth E. J., Hutchinson D. P., Nanos G. P., Jr, Partridge R. B., Wilkinson D. T., 1972, ApJ, 175, 217
Cocke W. J., Disney M. J., Taylor D. J., 1969, Nature, 221, 525
Collins S., Shearer A., Stappers B., Barbieri C., Naletto G., Zampieri L., Verroi E., Gradari S., 2012, in Griffin R. E. M., Hanisch R. J., Seaman R., eds, Proc. IAU Symp. 285, New Horizons in Time Domain Astronomy. Cambridge Univ. Press, Cambridge, p. 296

Downloaded from http://mnras.oxfordjournals.org/ at Uni Padova Fisica Astronomia on May 9, 2014

Edwards R. T., Hobbs G. B., Manchester R. N., 2006, MNRAS, 372, 1549
Germanà C. et al., 2012, A&A, 548, A47
Golden A., Shearer A., Redfern R. M., Beskin G. M., Neizvestny S. I., Neustroev V. V., Plokhotnichenko V. L., Cullum M., 2000, ApJ, 363, 617
Gradari S. et al., 2011, MNRAS, 412, 2689
Groth E. J., 1975a, ApJS, 29, 431
Groth E. J., 1975b, ApJS, 29, 453
Hobbs G. B., Edwards R. T., Manchester R. N., 2006, MNRAS, 369, 655
Horowitz P. et al., 1971, ApJ, 166, L91
Karpov S., Beskin G., Biryukov A., Debur V., Plokhotnichenko V., Redfern M., Shearer A., 2007, Ap&SS, 308, 595
Lohsen E. H. G., 1981, A&AS, 44, 1
Lynds R., Maran S. P., Trumbo D. E., 1969, ApJ, 155, L121
Lyne A. G., Pritchard R. S., Graham-Smith F., 1988, MNRAS, 233, 667
Lyne A. G., Pritchard R. S., Graham-Smith F., 1993, MNRAS, 265, 1003
Lyne A. G., Hobbs G., Kramer M., Stairs I., Stappers B., 2010, Science, 329, 408
Middleditch J., Pennypacker C. R., Burns M. S., 1987, ApJ, 315, 142
Mignani R. P., 2011, Adv. Space Res., 47, 1281
Naletto G. et al., 2009, A&A, 508, 531
Nasuti F. P., Mignani R., Caraveo P. A., Bignami G. F., 1996, A&A, 314, 849
Nelson J., Hills R., Cudaback D., Wampler J., 1970, ApJ, 161, L235
Oosterbroek T., de Bruijne J. H. J., Martin D., Verhoeve P., Perryman M. A. C., Erd C., Schulz R., 2006, A&A, 456, 283
Oosterbroek T. et al., 2008, A&A, 488, 271
Papaliolios C., Carleton N. P., 1970, Nature, 228, 445
Romani R. W., Miller A. J., Cabrera B., Nam S. W., Martinis J. M., 2001, ApJ, 563, 221
Strader M. J. et al., 2013, ApJ, 779, L12
Zampieri L. et al., 2011, Adv. Space Res., 47, 365

APPENDIX A: TRANSFORMATION OF THE ψ-PHASES BETWEEN TWO DIFFERENT TEMPORAL GAUGES

In the following, $t_p(t)$ is the time of arrival of the main pulse at/after time t, while $(\hat{P}_{init}, \hat{t}_0)$ and (P_{init}, t_0) refer to the two different temporal gauges. As mentioned above, we assume that the pulsar period changes slowly in time and, as a consequence, the two reference periods $\hat{P}_{init}$ and P_{init} are not very different from the actual pulsar period and from each other ($|\hat{P}_{init}/P_{init} - 1| <$ phase bin). We define

$$\hat{\alpha}(t) = \frac{t_p - \hat{t}_0}{\hat{P}_{init}} = \frac{t_p - t_0}{\hat{P}_{init}} + \frac{\Delta t}{\hat{P}_{init}} \tag{A1}$$

$$\alpha(t) = \frac{t_p - t_0}{P_{init}} \tag{A2}$$

where $\Delta t = t_0 - \hat{t}_0$ and the fractional part of $\hat{\alpha}$ and α is measured as described in Section 3 (like the ψ phase). As the time of arrival of a single pulse determined in the two different temporal gauges is equal, from the previous equations we obtain:

$$\hat{\alpha}(t) = \frac{P_{init}}{\hat{P}_{init}}\,\alpha(t) + \frac{\Delta t}{\hat{P}_{init}} \tag{A3}$$

Considering that, modulo 1, it is $fr[\hat{\psi}] = fr[-\hat{\alpha}]$ and $fr[\psi] = fr[-\alpha]$, after some manipulations we get:

$$fr[\hat{\psi}] + (n - \hat{n} - \hat{\psi}_n) = u\,fr[\psi] - (u-1)\,n - \frac{\Delta t}{\hat{P}_{init}} - \hat{\psi}_n \tag{A4}$$

where $n = \mathrm{int}[(t_p - t_0)/P_{init}]$, $\hat{n} = \mathrm{int}[(t_p - \hat{t}_0)/\hat{P}_{init}]$, $u = P_{init}/\hat{P}_{init}$ and $\hat{\psi}_n$ is an integer shift needed to align phases between successive nights. Writing $\hat{n} = \mathrm{int}[(t_p - t_0)/\hat{P}_{init}] + \mathrm{int}[\Delta t/\hat{P}_{init}]$, we finally obtain:

$$fr[\hat{\psi}] + (n - \hat{n}' - \hat{\psi}_n) = u\,fr[\psi] - (u-1)\,n - v - \hat{\psi}_n \tag{A5}$$

where $v = \Delta t/\hat{P}_{init} - \mathrm{int}[\Delta t/\hat{P}_{init}] = fr[\Delta t/\hat{P}_{init}]$. The integer part of $\hat{\psi}$ measured from t_0 consists of two contributions, the integer difference between the two temporal gauges $(n - \hat{n}')$ and the integer shift $(-\hat{\psi}_n)$. Equation (A5) corresponds to equations (6) and (7).

The same equation can be derived asking that the true rotational phase ϕ of the pulsar is gauge-independent. From equations (8) and (9), we have:

$$\phi(t) = \hat{\psi}(t) + \frac{(t - \hat{t}_0)}{\hat{P}_{init}} \tag{A6}$$

$$\phi(t) = \psi(t) + \frac{(t - t_0)}{P_{init}} + N, \tag{A7}$$

By equating these two expressions for ϕ and using the quantities defined above, after some manipulations we obtain:

$$\hat{\psi} = fr[\psi] - (u-1)\left(\frac{t - t_0}{P_{init}}\right) - v + N', \tag{A8}$$

where N' is an integer. Adding and subtracting $u\,fr[\psi]$, we finally have:

$$\hat{\psi} = u\,fr[\psi] - (u-1)\left(\frac{t - t_0}{P_{init}} + fr[\psi]\right) - v + N'. \tag{A9}$$

Since $fr[\psi] = fr[-\alpha] = -fr[(t_p - t_0)/P_{init}]$, equation (A9) can be written as

$$\hat{\psi} = u\,fr[\psi] - (u-1)\left[\mathrm{int}\left(\frac{t - t_0}{P_{init}}\right) + fr\left[\frac{t - t_p}{P_{init}}\right]\right] - v + N'. \tag{A10}$$

In the assumptions stated above, it is $|u - 1| \ll 1$. So, we can neglect the second term in square brackets on the right hand side and equation (A10) reduces to equation (A5) ($\mathrm{int}[(t - t_0)/P_{init}] = \mathrm{int}[(t_p - t_0)/P_{init}] = n$).

This paper has been typeset from a TEX/LATEX file prepared by the author.

Downloaded from http://mnras.oxfordjournals.org/ at Uni Padova Fisica Astronomia on May 9, 2014